



Exploring the Potential of the Google Earth Engine (GEE) Platform for Analysing Forest Disturbance Patterns with Big Data

Tunahan Cinar^{1*}, Abdurrahim Aydin¹

1. Duzce University, Faculty of Forestry, Konuralp Campus, 81620 Düzce, Türkiye

*Correspondence Author: Tunahan Çınar

e-mail: tunahancinar@duzce.edu.tr

e-mail: aaydin@duzce.edu.tr

ORCID (Tunahan Çınar): 0000-0002-6473-0884

ORCID (Abdurrahim Aydin): 0000-0002-6572-3395

ABSTRACT

Climate change has led to various adverse consequences, with natural disasters being one of the most striking outcomes. Natural disasters negatively impact life, causing significant disruptions to the ecosystem. Prompt identification of affected areas and initiation of the rehabilitation process are imperative to address the disturbances in the ecosystem. Satellite imagery is employed for the rapid and cost-effective detection of damages caused by natural disasters. In this conducted study, the outputs of climate change wildfire, forest change detection, and drought analysis, have been examined, all of which worsens the impacts on the ecosystem. The analysis of drought involved using MODIS data, while Sentinel-2A satellite images were utilized to identify wildfire areas and changes in forested regions caused by windthrow. The research focused on Ganja, Azerbaijan, as the area for drought analysis. The driest June between 2005 and 2018 was assessed using the Vegetation Condition Index (VCI) in conjunction with data from the National Centers for Environmental Information (NOAA). At the Düzce Tatlıdere Forest Management Directorate, the Normalized Difference Red Edge Index (NDRE) was utilized between the years 2018 and 2019 to detect the changes occurring in forested areas due to windthrow. The NDRE synthetic band was added to satellite images for the years 2018 and 2019, and a Random Forest (RF) algorithm was employed to classify the data. The classification results were evaluated using Total Accuracy and Kappa statistics. The study includes the detection of the Normalized Burn Ratio (NBR) applied to determine the extent of the wildfire that occurred in the Solquca village of the Qabala region in Azerbaijan in 2021. According to the analysis of the VCI and NOAA, June 2014 was identified as the driest month in Ganja. In the Tatlıdere region, the analysis indicated that 4.22 hectares experienced reforestation, while 24 hectares experienced deforestation. The NBR analysis has revealed that ~1007 hectares of land were burned in the Solquca village of Qabala. The analyses conducted provide information regarding the use of satellite imagery in relation to changes in forest areas due to drought, wildfire, and windthrow.

Keywords: Drought; wildfire; forest change detection; big data analysis; Google Earth Engine.

Exploración del potencial de la plataforma de Google Earth Engine (GEE) para el análisis de patrones de perturbación forestal a través de macrodatos

RESUMEN

El cambio climático ha generado varias consecuencias adversas, con los desastres naturales como uno de los efectos más notables. Los desastres naturales impactan negativamente la vida y causan grandes daños en los ecosistemas. La identificación temprana de las áreas afectadas y el comienzo de los procesos de rehabilitación son necesarios para abordar los desajustes en los ecosistemas. Las imágenes satelitales se emplean para una detección rápida y eficaz de los daños causados por los desastres naturales. En este estudio se examinan los resultados de los incendios forestales por el cambio climático, la detección de los cambios en los bosques y el análisis de sequías, los cuales empeoran aún más los ecosistemas. El análisis de sequías se elaboró con información satelital MODIS, mientras que las imágenes satelitales de Sentinel-2^a se utilizaron para identificar las áreas de incendios forestales y los cambios en las regiones boscosas causados por el viento. El área para el análisis de las sequías se ubica en Ganja, Azerbaiyán. El mes de junio más seco entre 2005 y 2018 se evaluó con el Índice de Condición Vegetal y con información del Centro Nacional para la Información Ambiental. En el Directorado de Administración Forestal Düzce Tatlıdere se ejecutó la Diferencia Normalizada de Borde Rojo (NDRE, del inglés Normalized Difference Red Edge Index) entre los años 2018 y 2019 para detectar los cambios ocurridos en las áreas boscosas debido a los daños en árboles ocasionados por fuertes vientos. Luego se añadió una banda sintética NDRE a las imágenes satelitales para los años 2018 y 2019 y se empleó un algoritmo de bosques aleatorios para clasificar la información. Los resultados de clasificación se evaluaron con las estadísticas Precisión Total y Kappa. El estudio incluye la aplicación del Índice Normalizado de Área Quemada para determinar la extensión del incendio forestal que ocurrió en la villa de Solquca, en la región de Qabala, en Azerbaiyán, durante el 2021. De acuerdo con los análisis de Índice de Condición Vegetal y del Centro Nacional para la Información Ambiental, junio de 2014 fue identificado como el mes más seco en Ganja. En la región de Tatlıdere los análisis indican que 4.22 hectáreas experimentaron un proceso de reforestación, mientras que 24 hectáreas experimentaron deforestación. El Índice Normalizado de Área Quemada reveló que unas 1007 hectáreas de tierra se quemaron en el incendio de la villa de Solquca. Estos análisis realizados proveen de información relacionada al uso de imágenes satelitales en relación con los cambios en las áreas forestales debido a la sequía, los incendios forestales y los daños en bosques ocasionados por fuertes vientos.

Palabras clave: Sequía; incendio forestal; cambio en la detección forestal; análisis de datos; Google Earth Engine

Record

Manuscript received: 14/07/2023

Accepted for publication: 28/01/2024

How to cite this item:

Cinar, T., & Aydin, A. (2023). Exploring the Potential of the Google Earth Engine (GEE) Platform for Analysing Forest Disturbance Patterns with Big Data. *Earth Sciences Research Journal*, 27(4), 437-448 <https://doi.org/10.15446/esrj.v27n4.110128>

1. Introduction

In recent years, significant increases in natural disasters have been observed in conjunction with the process of climate change. This can be attributed to various factors, including extreme temperatures, increased wind speeds, and intense precipitation events (Trenberth, 2011; Rummukainen, 2012). Additionally, alterations in climate parameters have given rise to unnatural disasters, such as wildfires, influenced by both climatic shifts and human factors (Lan et al., 2021; Boegelsack et al., 2018). As a result of the increasing frequency of natural disasters, numerous ecosystems are being impacted, and the recovery process is proving to be time-consuming. Therefore, it is crucial to promptly detect areas affected by natural disasters and implement interventions as quickly as possible (Basher, 2006). Ground measurements are typically conducted to identify areas affected by natural disasters. However, these ground measurements can be time-consuming and economically costly. (Ali et al., 2016; Yu et al., 2018) Due to the disadvantages of ground measurements, satellite images are often preferred for the detection of areas affected by various natural disasters, primarily due to their efficiency and cost-effectiveness (Edney and Wood, 2021).

But significant difficulties can be encountered by computer systems during the processes of acquiring, storing, analyzing, and visualizing satellite images Liu (2015). Because satellite images fall within the big data category, they can pose significant challenges in terms of computer storage and processing (Krishnan and Gonzalez, 2015; Ma et al., 2015). For the resolution of these problems, various programming languages are employed. However, the programming languages used sometimes have limitations in conducting a limited number of analyses. To address these challenges, the Google Earth Engine (GEE) platform, utilizing cloud-based infrastructure, emerges as an effective solution. GEE facilitates ease in handling data by storing it in its own cloud environment, providing conveniences for numerous studies (Gorelick et al., 2017). Within GEE, there exists a vast database consisting of numerous satellite images, demographic data, and environmental parameters such as elevation and slope. GEE allows for easy accessibility to the database related to the areas under study, thereby providing a more straightforward opportunity for analysis. (Moore and Hansen, 2011; Zhao et al., 2021).

Thanks to the advantages provided by GEE, the location identification of natural disasters resulting from climate change, as well as the determination of the affected area's extent and environmental parameters, can be easily accomplished (Scheip and Wegmann, 2021; Amani et al. 2020). Thanks to the conveniences it provides, GEE has facilitated various studies related to natural disasters, including wildfire (Seydi et al., 2021; Tavakkoli Piralilou et al., 2022), detection

of pollutants gases in forest fires (Çınar et al., 2023), windthrow area detection (Çınar et al., 2023), drought analysis (Sazib et al., 2018; Khan and Gilani, 2021), and flood area detection (Moharrami et al., 2021; Mehmood et al., 2021).

With the anticipated increase in natural disasters accompanying climate change, the prompt detection and rehabilitation of affected areas are crucial for effective response. The straightforward identification of disaster-stricken areas and understanding their historical conditions highlights the temporal and economic significance of satellite imagery. In this study, the Vegetation Condition Index (VCI) derived from MODIS satellite images was employed to analyze drought trends in Ganja, Azerbaijan, between 2005 and 2018. The data obtained from NOAA, including temperature, precipitation, and humidity, were utilized to evaluate the results of the Vegetation Condition Index (VCI). For the detection of windthrow areas and the assessment of reforestation and deforestation processes, Sentinel-2A satellite imagery was utilized. Normalized Difference Red Edge (NDRE) was calculated from Sentinel-2A images and integrated as a synthetic band into the satellite imagery. The windthrow area was classified using Random Forest (RF), with drone images serving as a reference. Statistical evaluation was conducted using Kappa analysis and Overall Accuracy. Lastly, the wildfire that occurred in the village of Solquca in Qabala, Azerbaijan, in 2021 was identified using Sentinel-2A satellite images and the Normalized Burn Ratio (NBR). The NBR results were classified into High Severity, Moderate-high Severity, Low Severity, Moderate-low Severity, Unburned, and Enhanced Regrowth, Low (post-fire). This study illustrates the effective utilization of satellite imagery in monitoring and detecting natural disasters.

2. Material and Methods

2.1. Material

GEE platform was used in this research because it offers a wide variety of helpful capabilities for programming crucial studies in forestry-related applications. Figure 1. depicts the primary components of the GEE user interface. Access to libraries is provided via the API documentation part, while the script manager is used to handle the code mechanisms. File types like "shapefile" and "TIFF" can be uploaded through Asset management. Users can customize the image processing and script writing capabilities of the code editor to meet their needs. Any formatting mistakes in the code are shown in the Inspector window. The output console provides numerical data and graphical representations. Importing analyzed images is made easier, and transferring files to and from "Google Drive" is possible, all within the Task management section. GEE platform's general user interface is depicted here.

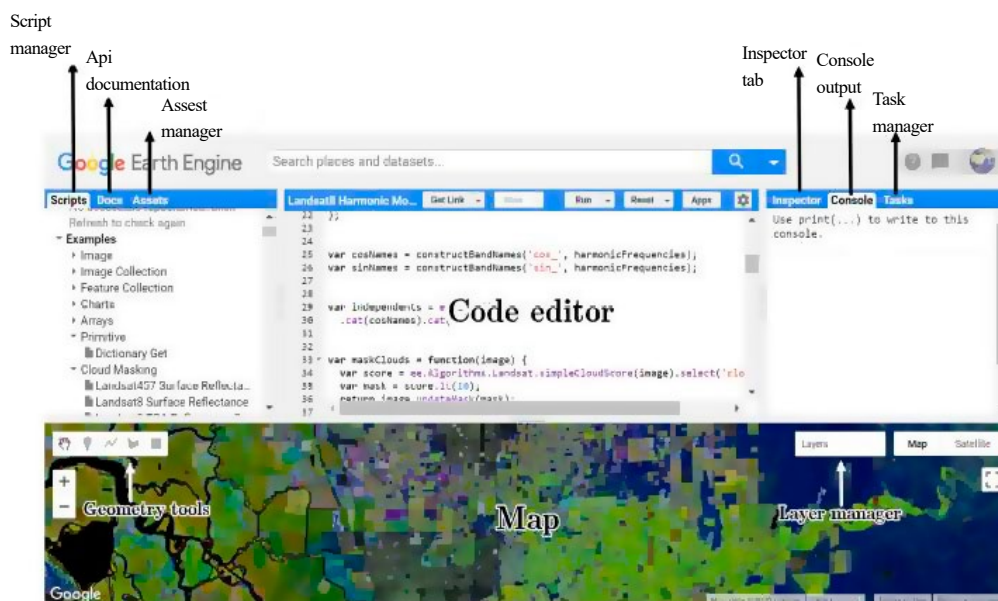


Figure 1. Google Earth Engine Platform Interface

2.2. Study areas

The research focused on specified regions for the purpose of analysis; the locations of these regions are shown in Figure 2. In the conducted study, Ganja was chosen for drought analysis. This selection was made because organic agriculture (Guliyeva and Lis, 2020; Aliyev et al., 2022) and forestry (Hasanov et al., 2020; Rosa, 2022) are significant economic livelihoods in Ganja. On the other hand, Tatlidere Forest Enterprise was chosen for the detection of reforestation and deforestation in windthrow areas due to the availability of drone images related to the damage in Düzce. The area selected for wildfire detection is the largest wildfire that occurred in Azerbaijan in 2021, specifically in the Qabala region. Abundance of forests in the Qabala region and the absence of research in the area influenced the choice of this region for the current study. The town of Ganja and the area immediately around it is located in the Kura-Aras Lowland ecoregion. This ecoregion is distinguished by its varied topography, which includes grasslands, shrublands, and riparian forests. Oak forests, wetlands, and grasslands can all be found within this region (Abbasov, 2018; Mammadov and Mammadov, 2016). Hasanov (2015) and Rahman et al. (2022) report that the region is put to use for agricultural and cultural pursuits respectively.

Windthrow study was carried out in the Tatlidere Forest Enterprise, which is situated in the city of Düzce in Türkiye. The area that was affected by the windthrow has the coordinates 31.357E - 40.865N and 31.373E - 40.851N in its corner points. The climate of the Tatlidere region, which is located in the Black Sea region of Türkiye, is characterized by high levels of both precipitation and humidity on average. The windthrow region is dominated by oak species and Eastern beech, scientifically known as *Fagus orientalis* Lipsky.

The province of Soqluca within the Qabala region, which is located in the northern section of Azerbaijan, served as the primary focus of the wildfire investigation that was carried out as part of this study. The Greater Caucasus Mountains can be seen in the distance from this region, which is found in their foothills. According to the Koppen climate classification system, Qabala has what is known as a humid subtropical climate, or Cfa for short. The region is

characterized by warm summers and chilly winters, and it receives a significant amount of precipitation throughout the course of the entire year (Aliyeva et al., 2020; Aliyev, 2005). The Qabala Region is made up of mountainous terrain that is covered in forest, as well as mountain meadows and rivers. According to Aliyeva et al. (2020), the woods in the area are distinguished by the presence of both deciduous and coniferous tree species, including oak, beech, and fir.

2.3. Data used

This study made use of MODIS (Moderate Resolution Imaging Spectroradiometer) satellite data, which was made available on the GEE platform, in order to undertake the drought analysis that was carried out in Ganja, Azerbaijan. MODIS is an integral instrument that is mounted on both the Terra and Aqua satellites that are part of NASA's Earth Observing System (EOS). The major goal of this instrument is to collect worldwide measurements of land, ocean, and atmospheric variables at a resolution that is somewhere between moderate and high. The visible through the thermal infrared spectrum is covered by the 36 spectral bands that are a part of the MODIS instrument. Depending on the particular spectral band, the device is capable of providing data at a variety of resolutions, ranging from 250 meters all the way up to 1 kilometer. Due to the fact that it has a swath width of 2330 km, it is able to acquire footage of the entire planet in as little as one or two days.

In addition, the GEE platform utilized Sentinel-2A imagery for coding forest degradation in the windthrow area of Duzce and wildfire study in the Solluca town of Qabala. Both of these activities took place in Qabala. As a part of the Copernicus programme, the European Space Agency (ESA) successfully launched a satellite known as Sentinel-2A in the year 2015. High-resolution land observation is its primary purpose, and it is outfitted with a multispectral imaging device known as the Multispectral device (MSI). The satellite has a swath width of 290 kilometres and a revisit period of 5 days at the equator, thus it can provide frequent coverage. Additionally, the satellite has a revisit time of 5 days.

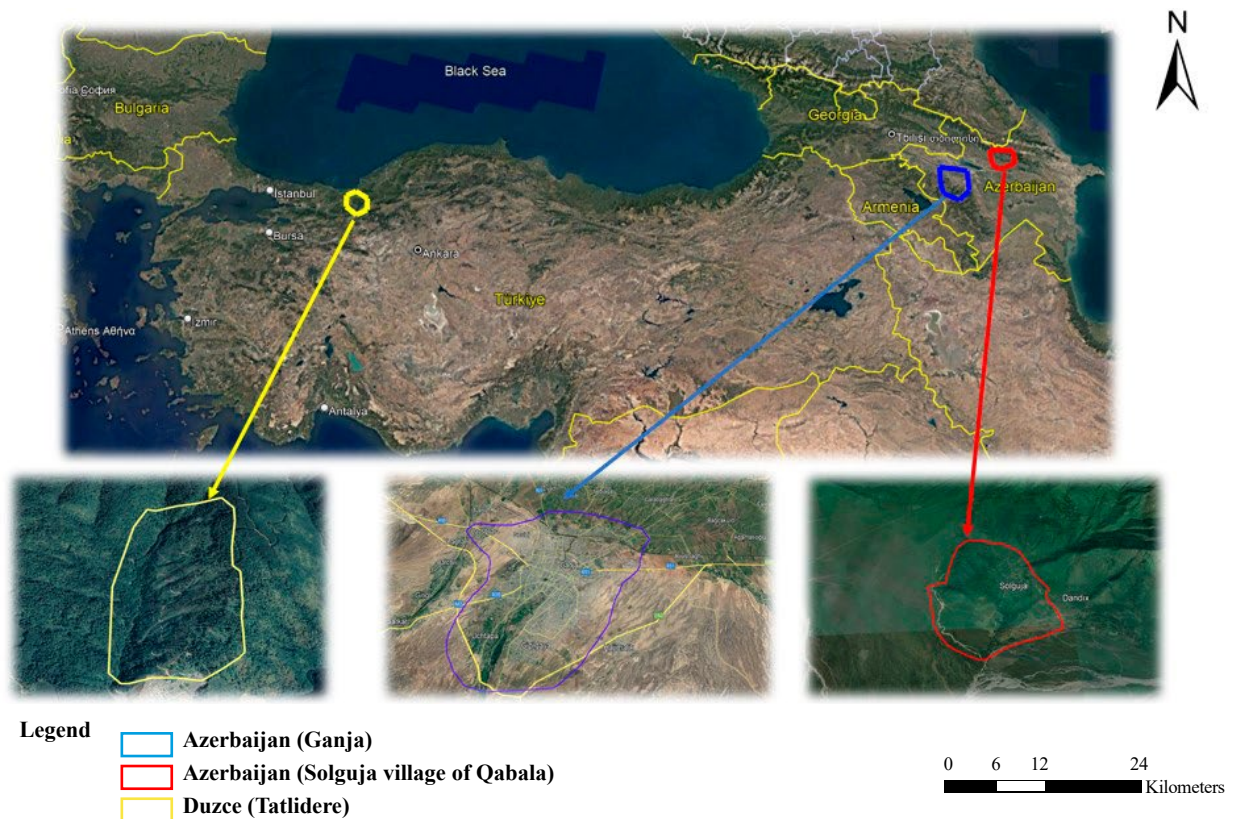


Figure 2. Location Map

2.4. Method

For the purpose of the present research, the GEE platform was utilized for the coding of forest area changes brought on by windthrow, to identify and evaluation of the impact of wildfire areas, and drought assessments. The process of coding was carried out within the GEE platform, making use of discrete procedures for the decoding of Earth observation imagery that were unique to each investigation. Figure 3 depicts the workflow that must be followed in order to carry out these analyses.

2.4.1 Drought Analysis

It is anticipated that changes in the climate would bring about a general warming of the planet as well as sudden increases in the speed of the wind. It is anticipated that the rise in temperatures caused by global warming would add to the worsening of drought conditions. In addition, trees, which play a significant part in reducing the negative effects of environmental change, may be put at risk of deterioration as a result of the growing wind speeds. One such predicted effect is an increase in the number of wildfires around the world that are caused by unexpected jumps in temperature.

The Vegetation Condition Index (VCI) was utilized in order to carry out the task of assessing the severity of the drought. The formula for the VCI, which is one of the indexes that is utilized, can be found in (1).

$$VCI = (X - X_{min}) / (X_{max} - X_{min}) * 100 \quad (1)$$

In this context, X stands for the smoothed weekly absolute Normalized Difference Vegetation Index (NDVI), (X_{max}) denotes the value of the multi-year NDVI that was highest, and (X_{min}) is the value of the multi-year NDVI that was lowest. According to Kogan (1995), Kogan and Sullivan (1993), the value of the VCI can range from zero to one hundred, with higher values indicating healthier vegetation environments and lower values representing vegetation that is stressed. VCI values are broken down into the following categories according to the classification constructed by Jain et al. (2009):

- Values of the VCI between zero and ten demonstrate a very dry condition.

- Values of the VCI between ten and twenty suggest that there is an extreme drought.
- Values of the VCI falling from twenty to thirty determine an average drought.
- Values of the VCI from thirty to forty indicate a moderate degree of drought.
- VCI scores that are higher than forty imply that there is no sign of drought.

The VCI plays a crucial role in the agribusiness and forestry industries by monitoring crop health and detecting signs of drought stress. It is also a valuable tool for evaluating the impact of environmental changes on vegetation and assessing ecosystem health. In regions where ground-based tracking is challenging, the VCI offers numerous advantages. Dutta et al. (2015) emphasize its effectiveness in efficiently managing plant health and drought-induced stress, enabling informed decision-making.

In the current research, a time series analysis was utilized so that the temporal fluctuations in the VCI could be analyzed. This analytical technique offers insightful understanding into the ways in which the VCI has changed throughout the course of time. The finds that were acquired from this analysis help in the process of interpretation because the data are represented visually in the results. The analysis of time series can be applied to many different data layers, as long as those data layers display temporal changes and include both historical and up-to-date information. (Liao, 2005; Wang et al., 2012) This methodology has seen extensive use across a variety of research domains, including environmental science and remote sensing, with the goal of investigating and better comprehending dynamic factors.

The findings of the time series analysis conducted on the VCI were validated using temperature and precipitation data obtained from the esteemed National Oceanic and Atmospheric Administration (NOAA) dataset. The NOAA satellite is used to detect atmospheric and climatic parameters. With NOAA, temperature, precipitation, and various ground measurements can be conducted. Due to its real-time representation of atmospheric events, NOAA is widely utilized in numerous research studies (Los et al., 2000; Hill et al., 2005; Engebretson et al., 2015).

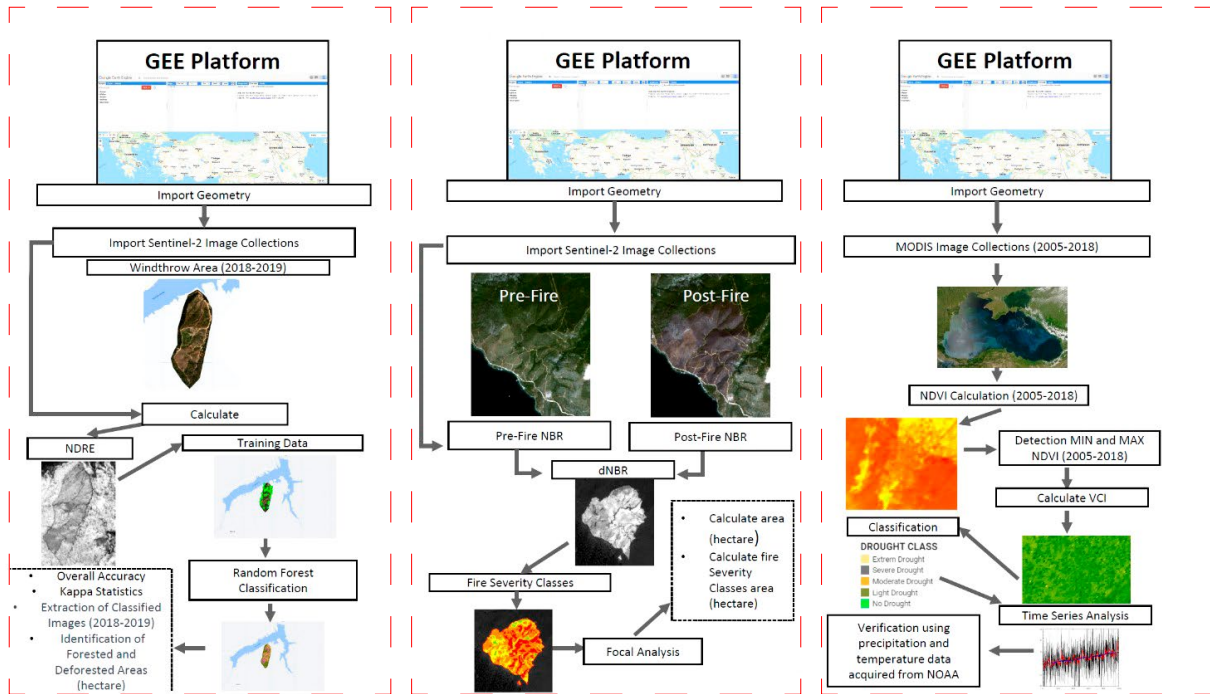


Figure 3. Workflow (The left-hand side of the visualization represents Forest area change due to windthrow, the middle part represents Wildfire, and the right-hand side represents Drought in the flowchart)

2.4.2. Detection of Changes in Forest Area Due to Windthrow Damage

The Normalized Difference Red Edge Index (NDRE) was utilized so that changes in forest area that were the result of windthrow could be assessed. (2) provides the formula that must be used in order to calculate the NDRE.

$$\text{NDRE} = (\rho_{\text{NIR}} - \rho_{\text{RE}}) / (\rho_{\text{NIR}} + \rho_{\text{RE}}) \quad (2)$$

The NDRE is a vegetation indicator that is an essential component of the algorithm that determines the rates of deforestation and reforestation. It does this by using reflectance values, which are affected by the amount of water and chlorophyll that are present in the leaves. According to Eitel et al. (2011), the NDRE index is a standard tool for evaluating the dynamics of vegetation and determining the level of stress present in plant and tree communities. Additionally, the NDRE index is capable of capturing reflected radiation, which can vary based on the particular properties of the plant species that are being investigated (Li et al., 2014).

For classification purposes, the area was divided into two categories: forested areas and regions with windthrow damage, with the drone image (Figure 6) of the area serving as a reference. The NDRE synthetic band has been added to the Sentinel-2A satellite image. Bands B2, B3, B4, B5, B6, B7, B8, and NDRE from the Sentinel-2A satellite image are utilized in the classification process. The importance values of the bands used in the classification have been determined according to the RF method. RF method is widely used in the field of machine learning. Through machine learning, it is possible to create specific classes within a database. RF can successfully apply the classification it has created and determine its effectiveness. In RF, training data is crucial, as it uses the provided training data to create trees within itself, aiming to achieve the best outcome. During the process of creating each tree, the RF algorithm generates random trees and separates them from each other based on the Gini index criterion. This allows it to provide the best possible result to the user. This random feature selection helps to prevent overfitting and encourages diversity among the trees, which ultimately contributes to an improvement in the random forest's overall performance. RF generates a robust prediction that demonstrates better accuracy and generalization capabilities. This is accomplished by integrating the outputs of a number of different trees. (Breiman, 1996). In Random Forest (RF), "mtry" represents the number of randomly selected features (predictor variables) at each split point when building decision trees within the ensemble. It is used to create decision trees within the forest. The "mtry" parameter in the RF algorithm determines the subset of features to be considered at each decision point (Genuer et al., 2008). A smaller "mtry" value introduces more randomness since fewer features are taken into account at each split, providing increased diversity among the individual trees in the forest. Therefore, the performance of the Random Forest (RF) model was assessed using a cross-validation dataset by running various "mtry" values. Efforts were made to determine the optimal "mtry" value in order to achieve the best results, and this value was determined to be "5."

Gini index is a metric that is utilized in order to evaluate the efficacy of a split that is contained within a decision tree. According to Breiman (1996), it is a method for quantifying the probability of incorrectly classifying a randomly picked element from a set if the element were labeled randomly. This method is based on the distribution of labels within the subset. Following is the formula that may be used to determine the Gini index value (3):

$$\sum \sum_{(j \neq i)} (f(K_i, M) / |M|) (f(K_j, M) / |M|) \quad (3)$$

The probability that the selected states belong to the class K_i is calculated using the expression $(f(K_i, M) / |M|)$, while the likelihood that they belong to the class K_j is expressed by the equation $(f(K_j, M) / |M|)$. Because of this scenario, the selected instances will contain members of many classes (Pal, 2005).

In the accuracy assessment stage, Kappa analysis, which is a widely utilized approach (Jensen et al., 1995; Foody, 2020), was employed. Kappa analysis is a statistical technique that assesses the agreement level between data sets and quantifies accuracy through a measure known as Kappa (Congalton, 1991; Rwanga and Ndambuki, 2017). The Kappa formula (4) is utilized to conduct this analysis.

$$\text{Kappa} = (Po - Pe) / (1 - Pe) \quad (4)$$

where:

Po is calculated by dividing the total number of observations by the number of observed agreements.

Pe = equals the "Expected Probability of Coincidence"

In categorical data, the level of agreement between observers or raters can be determined with the use of kappa values. The values of kappa can range anywhere from -1 to 1, and each value has a unique connotation depending on its value:

- If the kappa value is -1, it indicates that the observers are totally in agreement with each other. This indicates that the ratings present a perfect example of an inverted relationship, as well as a contradiction.
- A kappa value of 0 implies that the agreement was the result of random chance. In this instance, the observed agreement is quite comparable to what one would anticipate based just on the operation of random chance.

The level of agreement between the observers is considered to be flawless when the kappa value is 1. This indicates that there is perfect concordance between the evaluations, often known as consistency.

The interpretation of kappa values gives us the ability to understand the level of agreement that goes above what would be expected as a result of random chance. It offers a quantitative measure of agreement or disagreement, which gives researchers the capacity to evaluate the dependability or consistency of categorical data evaluations. (Gwet, 2002; Sim and Wright, 2005).

When evaluating the precision of a classification or prediction model, one metric that is commonly used is called the Overall Accuracy. According to Alberg et al. (2004) and Sui et al. (2014), it is the ratio of correctly classified samples or observations to the total number of samples or observations in the dataset. The following is the formula for the overall accuracy score (5):

$$\text{Overall Accuracy} = (\text{Number of correctly classified samples} / \text{Total number of samples}) \times 100 \quad (5)$$

Overall Accuracy values fall within the range of 0 to 100, where a value of 0 implies no correct classifications, while a value of 100 indicates that all classifications are accurate.

The values for the Overall Accuracy range from 0 to 100, where a value of 0 indicates that there are no correct classifications and a value of 100 indicates that all classifications are accurate (Mellor et al., 2013).

2.4.3. Wildfire Area Detection from Sentinel-2A Satellite Imagery

The Normalized Burn Ratio (NBR) was calculated on the Sentinel-2A satellite imagery to identify wildfire-affected areas using satellite imagery (Lopez et al., 1991). The formula to calculate this index using the satellite image is provided in the following number: (6).

$$\text{NBR} = (\rho_{\text{NIR}} - \rho_{\text{SWIR}}) / (\rho_{\text{NIR}} + \rho_{\text{SWIR}}) \quad (6)$$

The bands in the satellite image that are represented by NIR and SWIR correspond to specific wavelengths, such as B8 and B12 in Sentinel 2A. The NBR was computed using the satellite image that was captured both before and after the fire, and the area of the wildfire was determined by applying equation (7) (Lasaponara et al., 2019).

$$\text{dNBR} = (\text{NBR}_{\text{prefire}} - \text{NBR}_{\text{postfire}}) \quad (7)$$

The NBR analysis results derived from Sentinel-2A satellite imagery have been subjected to classification. The following bands value were used to define the categories: values between +660 and +1300 indicate "High Severity," whereas values between +440 and +659 indicate "Moderate-high Severity,"

values between +270 and +439 indicate “Low Severity,” values between +100 and 269 indicate “Unburned,” values between -100 and -99 indicate “Enhanced Regrowth, Low,” and values between -250 and -101 indicate “Enhanced Regrowth, High” (Key and Benson, 2006).

3. Results

3.1. Drought monitoring through VCI

Ganja was selected as the research region to conduct drought analysis, and the borders of the area were outlined on the GEE platform using a geometric shape. A total of 301 NDVI photos were analyzed in order to determine which June in the region experienced the lowest amount of precipitation between the years 2005 and 2018. After doing some calculations, the satellite image’s minimum, maximum, and overall NDVI values were found. NDVI pictures were used in the calculation of the VCI, after which the appropriate formula was applied in order to generate a single image. After that, the resulting VCI image was categorized by assigning various colors to each class, and the results of that classification were displayed in the legend. According to the findings of the study, the month of June in the Ganja region had a drought during the year 2014. This was determined based on the data. The results of the VCI drought analysis are presented in Figure 4.

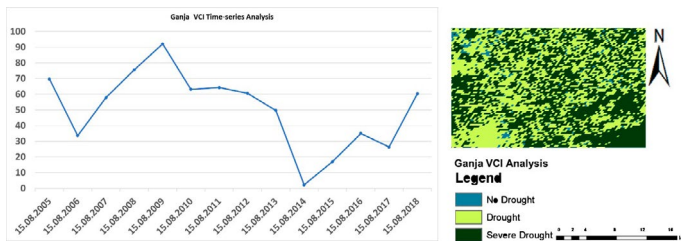


Figure 4. The result of the VCI drought index analysis

The results of the time series analysis are displayed on the console screen (Figure 4), which may be found here. The blue line in the graph reflects the changes in drought levels over time as indicated by the VCI index. The data points in the graph indicate the individual days on which these circumstances were observed. The specified region was determined to be experiencing a severe drought in June 2014 by using the VCI index.

In order to verify the findings of the VCI, weather information for Ganja during the driest June that occurred between 2005 and 2018 was retrieved from the NOAA and showed in Table 1. The highest temperature ever measured in June was 27.9 °C in both 2014 and 2016, while 2014 also saw the least amount of precipitation with only 1 millimeter falling during that month. On the other hand, the year 2009 was marked by the highest total quantity of precipitation ever recorded, which came in at 23.1 millimeters. In addition to precipitation (mm) and temperature (°C), the humidity (%) levels between June 2005 and 2018 were also determined from NOAA data. According to NOAA data the minimum humidity level was recorded in 2014 at 1% while the maximum humidity levels were detected in 2009 and 2010 at 14%. The data provided by the NOAA indicate that the month of June 2014 was classified as a drought year because of the significant disparity between the average temperature, amount of precipitation and the humidity. The VCI time series analysis, which was performed using MODIS satellite imagery, came to the conclusion that June 2014 was the driest month ever recorded.

3.2. The detection of reforestation and deforestation area changes due to windthrow

Within a windthrow area during the course of a single year, this study made use of Sentinel-2A photos to identify places that have undergone reforestation as well as deforestation. The major purpose of the method was to provide an estimation of the size of these regions expressed in hectares. The algorithm

consisted of a few different phases. To begin, NDRE values were determined by using the satellite photos that were obtained in the months of June 2018 and June 2019. Subsequent to this step, the RF classification, based on the drone imagery (Figure 5.), was applied to satellite photographs taken in the same month for both regions. Overall Accuracy and Kappa Statistics were utilized in the process of determining whether or not the categorization was accurate.

Figure 6. on the GEE platform provides a graphical representation of the findings of the investigation.



Figure 5. The drone imagery of the area affected by windthrow damage

Table 1. Average precipitation, temperature and humidity NOAA (2005-2018)

Date	Precipitation (mm)	Temperature (°C)	Humidity (%)
2005	11	22.8	7
2006	18	20.1	9
2007	7	26.3	5
2008	18	26.7	9
2009	27	23.1	14
2010	23	26.5	14
2011	4	25.1	2
2012	2	26.9	2
2013	18	24.6	10
2014	1	27.4	1
2015	2	26.7	2
2016	6	27.9	4
2017	6	27.1	4
2018	16	25.6	9



Figure 6. Result of deforestation algorithm (windthrow) analysis

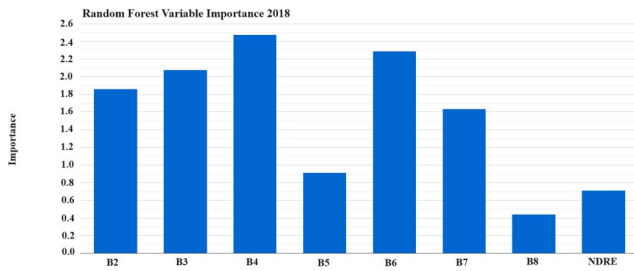


Figure 7. Importance values for the classified bands in the Sentinel-2A satellite imagery from the year 2018.

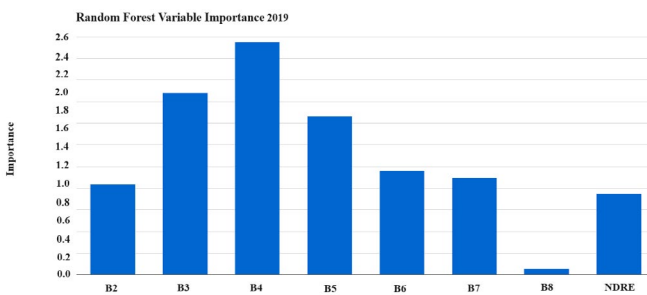


Figure 8. Importance values for the classified bands in the Sentinel-2A satellite imagery from the year 2019.

According to the findings of the study, there was reforestation in an area of roughly 4.22 hectares between the years 2018 and 2019, but there was also deforestation in an area of approximately 24 hectares during that same time period. According to the data that was collected, reforestation accounted for 0.95% of the total area, whereas deforestation affected 5.39% of the land, and the remaining 93.66% of the area did not change. Both the 2018 and 2019 satellite photos showed promising performance when it came to the accuracy evaluation of the classification results. It was discovered that the total accuracy of the image for 2018 was found to be 92.2%, which indicates a high level of agreement between the secret image and the data collected from the ground.

This would imply that the classification model was successful in capturing the various land cover classifications to an acceptable level of accuracy. For the picture from 2018, the Kappa statistic, which gauges agreement, came out to be 0.84 when it was calculated. This score demonstrates a significant level of agreement and adds even more weight to the validity of the classification outcomes. The Total Accuracy was calculated to be 93.75% for the satellite picture that was acquired in 2019, which, when compared to the image that was acquired in 2018, indicates a marginal improvement in accuracy. The Kappa Statistic for the 2019 image was calculated to be 0.85, which once again demonstrates a significant level of agreement between the two sets of data. The importance graph of the bands for the Sentinel-2A satellite images classified by the RF method in the years 2018-2019 is provided in Figure 7. and Figure 8.

In the classification results based on Sentinel-2A for the years 2018-2019, the most crucial band for classification was found to be B4 (RED) within the wavelength range of 0.665-0.705 µm. On the other hand, B8 (Vegetation Red Edge) within the wavelength range of 0.783-0.842 µm contributed the least to the classification.

3.3. Wildfire area mapping and assessment

For the purpose of this study, imagery obtained from the Sentinel-2A satellite was analyzed to locate areas affected by wildfires. In order to determine which regions were burned, the NBR index was applied in the form of coding. Before computing the NBR index, cloud masks were applied to both pre-fire and post-fire satellite pictures. This was done to guarantee that the results were accurate. This procedure serves to reduce the influence that cloud cover has on the results of the analysis. The generated NBR index photos were separated into pre-fire and post-fire images while they were being processed by the GEE platform. It was possible to exactly calculate the size of the region that was affected by the wildfire by using the equation (NBR prefire-NBR postfire) to subtract the NBR value of the image that was taken before the fire from the NBR value of the image that was taken after the fire. This approach makes it possible to identify and map the precise regions that were impacted by the wildfire. This approach provides vital information that can be used for further analysis and management purposes. Wildfire area recognition is made more accurate and efficient thanks to the integration of satellite data, the NBR index, and approaches for cloud masking into the GEE platform.

We followed the scale that was presented in Figure 9., which was initially devised by Key and Benson (2006), in order to classify the wildfire area that was found. Figure 10. provides a graphical representation of the extensive findings that were derived from our examination and was received from the GEE platform.

	Severity Level	dNBR Range (scaled by 10^3)	dNBR Range (not scaled)
	Enhanced Regrowth, high (post-fire)	-500 to -251	-0.500 to -0.251
	Enhanced Regrowth, low (post-fire)	-250 to -101	-0.250 to -0.101
	Unburned	-100 to +99	-0.100 to +0.99
	Low Severity	+100 to +269	+0.100 to +0.269
	Moderate-low Severity	+270 to +439	+0.270 to +0.439
	Moderate-high Severity	+440 to +659	+0.440 to +0.659
	High Severity	+660 to +1300	+0.660 to +1.300

Figure 9. The severity levels of burning

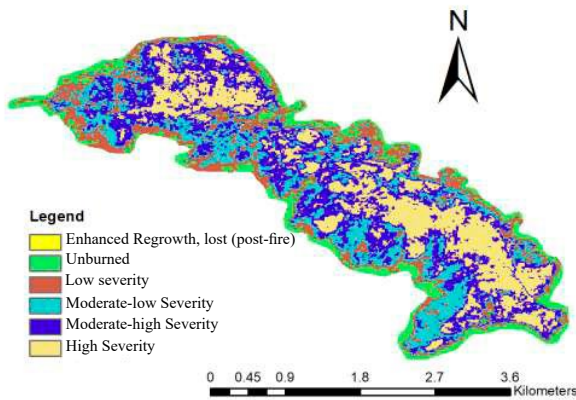


Figure 10. The result of the NBR index analysis

According to the findings of the investigation into the NBR index, the wildfire was responsible for the destruction of approximately ~1,007 hectares of land. In particular, the evaluation found that about ~219 hectares were categorized as “High Severity,” ~262 hectares were classified as “Moderate-high Severity,” and the remaining hectares were classified as “Low Severity.” ~194 hectares were classified as having “Moderate-low Severity,” while ~332 hectares were classified as having “Unburned and Enhanced Regrowth, Low (post-fire).”

4. Discussion

During this period of increased frequency in natural disasters, numerous regions are experiencing damage. It is imperative to promptly identify the affected and damaged areas, initiating the rehabilitation process swiftly. The most time-efficient method for identifying damaged areas and monitoring the recovery process is through satellite imagery. In recent times, cloud-based approaches have gained prominence, facilitating faster analysis by alleviating the impact of satellite imagery on computer storage capacity. In this study, the GEE platform, utilizing cloud storage, has been chosen for its advantages in enabling efficient analysis and processing. Within GEE, it is possible to observe various interdisciplinary studies such as land cover mapping (Huang et al., 2017), vegetation monitoring (Li et al., 2020), land use change detection (Adelisaridou et al., 2021), forest carbon mapping (Kafy et al., 2023), urban land cover analysis (Sidhu et al., 2018), and evaluating large-scale environmental initiatives (Lin et al., 2020). In addition to these analyses, GEE can also be applied to studying natural disasters such as wildfires (Tavakkoli Piralilou et al., 2022) and drought analysis (Khan and Gilani, 2021). In this study, analyses

have been conducted on drought, wildfire area detection, and forest change detection due to windthrow.

For drought analysis, indices such as the Temperature Condition Index (TCI) and Vegetation Health Index (VHI) can be used. However, in the mentioned study, Vegetation Condition Index (VCI) was employed to identify the driest month of June. The preference for using VCI in drought analysis is based on a study by Zhong et al. (2020), which stated that VCI values increase during the vegetation development process but decrease outside the vegetation periods. The study emphasized the usefulness of the Vegetation Condition Index (VCI) in drought analysis by highlighting its strong correlation with precipitation and temperature, excluding the vegetation periods. In another study utilizing VCI, Niu et al. (2022) used MODIS satellite imagery. They emphasized the high correlation between VCI and precipitation as well as temperature in the Pearl River Basin, and highlighted its strong relationship with soil moisture. In a different study, Dai et al. (2022) stated that VCI values increase during vegetation development periods. They also emphasized the significant correlation between VCI and temperature, noting that VCI decreases with rising temperatures and reduced rainfall. Based on the collective evidence from these studies in the literature, it can be concluded that VCI serves as a promising indicator of drought.

Monitoring the temporal changes in drought is of great importance due to the anticipated increase in drought occurrences as a consequence of climate change, which can have detrimental effects on forest areas and other natural habitats. In this coding study, the Vegetation Condition Index (VCI) was calculated and time series analysis was performed to detect variations in drought over the years. Other researchers, such as Zhao et al. (2021), Khan and Gilani (2021) and Zhao et al. (2022), have conducted similar studies; however, these investigations were conducted in different countries. Notably, Rezaei et al. (2014) previously employed the VCI in a study conducted in Azerbaijan to determine drought levels. Their research focused on Sharghi and identified drought years between 2000 and 2011, highlighting the highest drought levels in 2000, 2001, 2008, and 2009. However, their study did not include an analysis of drought trends over the years and was limited by the absence of local weather station data. In contrast, this present study, conducted in Ganja province, utilized two distinct data sources to assess drought levels. According to the VCI analysis, the driest month in Ganja was June 2014. The results of the analysis, based on temperature, precipitation and humidity parameters obtained from NOAA, are supportive of each other.

Another analysis conducted in the study is the identification of wildfire areas. The studies conducted by Parks et al. (2018), Arruda et al. (2021), and Konkathi and Shetty (2021) can be observed regarding the detection of wildfire areas on the GEE platform. Parks et al. (2018), Arruda et al. (2021), and Konkathi and Shetty (2021) utilized the Normalized Burn Ratio (NBR) to identify wildfire areas. They emphasized the ability of NBR to rapidly and accurately detect wildfire areas within defined boundaries. In our GEE wildfire area detection study, we also employed NBR. According to the NBR results, we determined that approximately ~1007 hectares of land in the Solquca village of Qabala were affected by wildfires. In a research conducted by Konkathi and Shetty (2021), utilizing NBR, it was stated that a total of ~78,000 hectares of land in the Kudremukh National Park in the Western Ghats of India were affected by wildfires. Another study using NBR, conducted by Parks et al. (2018), emphasized the successful detection of 18 different wildfires in the United States. They found that the average size of the wildfires was ~15,000 hectares. In a different study, Arruda et al. (2021) identified a total area of ~20,223 hectares affected in the Brazilian savanna using NBR. Arruda et al. (2021) emphasized the reliability of NBR by stating that it detected 97% of the fire-affected area in their study. Parks et al. (2018), Arruda et al. (2021), and Konkathi and Shetty (2021) have reported wildfire sizes in their respective studies that are larger than the affected area in Solquca village of Qabala. In contrast to other studies Parks et al. (2018), Arruda et al. (2021), and Konkathi and Shetty (2021), this study incorporated the use of “Focal Statistics” after NBR classification to calculate the statistics of each cell in relation to its neighboring cells, thus minimizing pixel misclassification. The use of Focal Statistics can contribute to the establishment of more precise boundaries and more accurate results for burnt areas. According to the results obtained from the application of Focal Statistics, the wildfire in Qabala was categorized into various severity classes: ~219 hectares were classified as high severity,

~262 hectares as moderate-high severity, ~194 hectares as moderate-low severity, and ~332 hectares as low severity.

In this study another analysis, changes in forested areas affected by windthrow were detected by calculating the NDRE and applying classification based on RF. The classification was validated using the areas identified in the drone imagery as a reference. While previous studies by Schmid (2017) and Brovelli et al. (2020) employed the Normalized Difference Vegetation Index (NDVI) in the study to explore forest change areas, this study used the NDRE index to assess changes in forest areas resulting from windthrow. The decision to use NDRE was influenced by the findings of Minařík and Langhammer (2016), who highlighted its superior boundary delineation capabilities in damaged forest areas. This choice was further supported by Einzmann et al. (2017), who identified NDRE as one of the most suitable indices for windthrow-affected areas. Additionally, Reinisch et al. (2020) demonstrated the effectiveness of NDRE in detecting deforestation impacts on vegetation, indicating its potential as a valuable tool for monitoring land-use change effects on ecosystems. Sharifi and Felegari (2023) also confirmed the higher sensitivity of NDRE compared to NDVI in assessing changes in vegetation health and biomass. For the satellite image classification, the RF classification technique was employed in this study. The preference for RF was based on the studies conducted by Sheykhoua et al. (2020), Na et al. (2010), and Zhang and Yang (2020), which demonstrated the superior performance of RF compared to other classification methods such as Support Vector Machine (SVM) and CART. RF exhibited higher accuracy in the classification results. The classification results using RF showed an overall accuracy of 92.2% and a Kappa statistic of 0.84 for the 2018 satellite image. Similarly, for the 2019 image, the overall accuracy was 93.75% with a Kappa statistic of 0.85. These statistical results indicate a high level of reliability in the classification results, falling under the “Almost perfect agreement” category as defined by Viera and Garrett (2005). The classification of images showing windthrow-induced changes in forests, categorized under “Almost perfect agreement,” demonstrates the efficacy of the NDRE index in detecting changes in forested areas affected by windthrow.

5. Conclusions

Climate change is causing serious disruptions to natural ecosystems. The disturbances in natural ecosystems lead to global water scarcity, followed by the emergence of drought issues. Additionally, there is a significant increase in forest fires, another natural disaster, observed worldwide. Climate change has resulted in changes in certain climate parameters. One of the parameters undergoing changes is wind speed. Sudden increases in wind speed can create serious disruptions in ecosystems. It is crucial to detect and initiate the rehabilitation of ecosystem disturbances as soon as possible. To commence rehabilitation, it is necessary to promptly identify the damaged areas. Satellite images are the most suitable tool for identifying damaged areas in the most cost-effective and time-efficient manner. However, the processing time for satellite images can be lengthy. The processing can be expedited by implementing specific algorithms and platforms. One of the platforms that shortens the processing time of satellite images is GEE. In this study, GEE was utilized for the analysis of natural disasters that have occurred in conjunction with climate change. Different algorithms were used for each analysis, and the results of the analyses were evaluated. This study specifically focused on the analysis of drought, wildfire, reforestation and deforestation area changes due to windthrow addressing disruptions in natural ecosystems. The study provides information on the detection of natural disasters in satellite images and the monitoring process.

Availability and Requirements

Drought Code: <https://code.earthengine.google.com/b7c272045e4c0de79124c8d312c445b5>

Forest Area Change due to Windthrow Code: <https://code.earthengine.google.com/e84759ded357047b9e751149d0bf600c>

Wildfire Areas Detection Code: <https://code.earthengine.google.com/063621b947fbcf6266175cb0cd06b9de>

References

- Abbasov, R. (2018). *Assessment of the Fresh Water Ecosystem Services of Reservoirs/HPP Dams in the Kura-Aras River Basin*. 17th World Lake Conference, Lake Kasumigaura, Ibaraki, Japan, 219.
- Adelisardou, F., Zhao, W., Chow, R., Mederly, P., Minkina, T., & Schou, J. S. (2021). Spatiotemporal change detection of carbon storage and sequestration in an arid ecosystem by integrating Google Earth Engine and InVEST (the Jiroft plain, Iran). *International Journal of Environmental Science and Technology*, 19, 5929–5944. <https://doi.org/10.1007/s13762-021-03676-6>
- Alberg, A. J., Park, J. W., Hager, B. W., Brock, M. V., & Diener-West, M. (2004). The Use of “Overall Accuracy” to Evaluate the Validity of Screening or Diagnostic Tests. *Journal of General Internal Medicine*, 19(5p1), 460–465. <https://doi.org/10.1111/j.1525-1497.2004.30091.x>
- Ali, I., Cawkwell, F., Dwyer, E., Barrett, B., & Green, S. (2016). Satellite Remote Sensing of Grasslands: from Observation to Management. *Journal of Plant Ecology*, 9(6), 649–671. <https://doi.org/10.1093/jpe/rtw005>
- Aliyev, L. A. (2004). Analysis of Radio Ecological Situation in Azerbaijan. In: Zaidi, M. K., & Mustafaev, I. (Eds.). *Radiation Safety Problems in the Caspian Region*. Nato Science Series: IV: Earth and Environmental Sciences, vol 41. Springer, Dordrecht. https://doi.org/10.1007/1-4020-2378-2_37
- Aliyev, S. T., Mammadova, E. B., Hamidova, L. A., Dunyamaliyeva, V. R., & Hushudov, S. N. (2022). Prospects and Threats for Developing Organic Agriculture: the Example of Azerbaijan. *Journal of Eastern European and Central Asian Research (JEECAR)*, 9(6), 1046–1054. <https://doi.org/10.15549/jeeecar.v9i6.1204>
- Aliyeva, G. N., Mammadova, Z. A., Ojaghi, J. M., & Pourbabaei, H. (2020). Inter- and Intrapopulation Variations in Leaf Morphological and Functional Traits of *Quercus petraea* ssp. *iberica* Under Ecological Factors in Azerbaijan. *Plant & Fungal Research*, 3(2), 61–68. <http://dx.doi.org/10.29228/plantfungalres.78>
- Amani, M., Ghorbanian, A., Ahmadi, S. A., Kakoei, M., Moghimi, A., Mir-mazloumi, S. M., ... & Brisco, B. (2020). Google Earth Engine Cloud Computing Platform for Remote Sensing Big Data Applications: A Comprehensive Review. *IEEE Journal of Selected Topics in Applied Earth Observations and Remote Sensing*, 13, 5326–5350. <https://doi.org/10.1109/JSTARS.2020.3021052>
- Arruda, V. L., Piontekowski, V. J., Alencar, A., Pereira, R. S., & Matricardi, E. A. (2021). An Alternative Approach for Mapping Burn Scars Using Landsat Imagery, Google Earth Engine, and Deep Learning in the Brazilian Savanna. *Remote Sensing Applications: Society and Environment*, 22, 100472. <https://doi.org/10.1016/j.rsase.2021.100472>
- Basher, R. (2006). Global Early Warning Systems for Natural Hazards: Systematic and People-Centred. *Philosophical transactions of the Royal Society A. Mathematical, Physical and Engineering Sciences*, 364(1845), 2167–2182. <https://doi.org/10.1098/rsta.2006.1819>
- Boegelsack, N., Withey, J., O’Sullivan, G., & McMartin, D. (2018). A Critical Examination of the Relationship Between Wildfires and Climate Change With Consideration of the Human Impact. *Journal of Environmental Protection*, 9(5), 461–467. <https://doi.org/10.4236/jep.2018.95028>
- Breiman, L. (1996). Bagging Predictors. *Machine Learning*, 24, 123–140. <https://doi.org/10.1007/BF00058655>
- Brovelli, M. A., Sun, Y., & Yordanov, V. (2020). Monitoring Forest Change in the Amazon Using Multi-Temporal Remote Sensing Data and Machine Learning Classification on Google Earth Engine. *ISPRS International Journal of Geo-Information*, 9(10), 580. <https://doi.org/10.3390/ijgi9100580>
- Congalton, R. G. (1991). Remote Sensing and Geographic Information System Data Integration: Error Sources and Research Issues. *Photogrammetric Engineering & Remote Sensing*, 57(6), 677–687.

- Çınar, T., Özdemir, S., & Aydin, A. (2023). Identifying Areas Prone to Windthrow Damage and Generating Susceptibility Maps Utilizing a Novel Vegetation Index Extracted from Sentinel-2A Imagery. *Journal of the Indian Society of Remote Sensing*, 51, 2391–2402. <https://doi.org/10.1007/s12524-023-01772-3>
- Çınar, T., Taşpinar, F., & Aydin, A. (2023). Analysis and Estimation of Gaseous Air Pollutant Emissions Emitted Into the Atmosphere During Manavgat and Milas Wildfire Episodes Using Remote Sensing data and Ground Measurements. *Air Quality, Atmosphere & Health*, 1-21. <https://doi.org/10.1007/s11869-023-01463-5>
- Dai, X., Yu, Z., Matheny, A. M., Zhou, W., & Xia, J. (2022). Increasing Evapotranspiration Decouples the Positive Correlation Between Vegetation Cover and Warming in the Tibetan Plateau. *Frontiers in Plant Science*, 1-13. <https://doi.org/10.3389/fpls.2022.974745>
- Dutta, D., Kundu, A., Patel, N. R., Saha, S. K., & Siddiqui, A. R. (2015). Assessment of Agricultural Drought in Rajasthan (India) Using Remote Sensing Derived Vegetation Condition Index (VCI) and Standardized Precipitation Index (SPI). *The Egyptian Journal of Remote Sensing and Space Science*, 18(1), 53-63. <https://doi.org/10.1016/j.ejrs.2015.03.006>
- Edney, A. J., & Wood, M. J. (2021). Applications of Digital Imaging and Analysis in Seabird Monitoring and Research. *Ibis*, 163(2), 317-337. <https://doi.org/10.1111/ibi.12871>
- Einzmann, K., Immitzer, M., Böck, S., Bauer, O., Schmitt, A., & Atzberger, C. (2017). Windthrow Detection in European Forests with Very High-Resolution Optical Data. *Forests*, 8(1), 21. <https://doi.org/10.3390/f8010021>
- Eitel, J. U., Vierling, L. A., Litvak, M. E., Long, D. S., Schulthess, U., Ager, A. A., ... & Stoscheck, L. (2011). Broadband, Red-Edge Information from Satellites Improves Early Stress Detection in A New Mexico Conifer Woodland. *Remote Sensing of Environment*, 115(12), 3640-3646. <https://doi.org/10.1016/j.rse.2011.09.002>
- Engebretson, M. J., Posch, J. L., Wygant, J. R., Kletzing, C. A., Lessard, M. R., Huang, C. L., ... & Shiokawa, K. (2015). Van Allen Probes, NOAA, GOES, and Ground Observations of An Intense EMIC Wave Event Extending Over 12 H in Magnetic Local Time. *Journal of Geophysical Research: Space Physics*, 120(7), 5465-5488. <https://doi.org/10.1002/2015JA021227>
- Foody, G. M. (2020). Explaining the Unsuitability of the Kappa Coefficient in the Assessment and Comparison of the Accuracy of Thematic Maps Obtained by Image Classification. *Remote Sensing of Environment*, 239, 111630. <https://doi.org/10.1016/j.rse.2019.111630>
- Genuer, R., Poggi, J. M., & Tuleau, C. (2008). Random Forests: Some Methodological Insights. *arXiv preprint arXiv:0811.3619*. <https://doi.org/10.48550/arXiv.0811.3619>
- Gorelick, N., Hancher, M., Dixon, M., Ilyushchenko, S., Thau, D., Moore, R. (2017). Google Earth Engine: Planetary-Scale Geospatial Analysis for Everyone. *Remote Sensing of Environment*, 202, 18–27. <https://doi.org/10.1016/j.rse.2017.06.031>
- Guliyeva, A. E., & Lis, M. (2020). Sustainability Management of Organic Food Organizations: A Case Study of Azerbaijan. *Sustainability*, 12(12), 5057. <https://doi.org/10.3390/su12125057>
- Gwet, K. (2002). Kappa Statistic is not Satisfactory for Assessing the Extent of Agreement Between Raters. *Statistical Methods for Inter-Rater Reliability Assessment*, 1(6), 1-6.
- Hasanov, A. A., Khan-Khoyskaya, I. V., & Bagirova, A. M. (2020). Natural and Resource Potential of the Region as Part of Investment Resources: Evidence from the Ganja-Gazakh Economic Region of Azerbaijan. *Digest-Finance*, 25(1 (253)), 17-29.
- Hasanov, E. L. O. (2015). Multidisciplinary Approach to Investigation of the Basic Handicraft Branches Of Ganja Till the XX Century. *Theoretical & Applied Science*, 1, 7-15.
- Hill, S. M., Pizzo, V. J., Balch, C. C., Biesecker, D. A., Bornmann, P., Hildner, E., ... & Zimmermann, F. (2005). The NOAA Goes-12 Solar X-Ray Imager (SXI) 1. Instrument, Operations, and Data. *Solar Physics*, 226, 255-281. <https://doi.org/10.1007/s11207-005-7416-x>
- Huang, H., Chen, Y., Clinton, N., Wang, J., Wang, X., Liu, C., ... & Zhu, Z. (2017). Mapping Major Land Cover Dynamics in Beijing Using All Landsat Images in Google Earth Engine. *Remote Sensing of Environment*, 202, 166-176. <https://doi.org/10.1016/j.rse.2017.02.021>
- Jain, S. K., Keshri, R., Goswami, A., Sarkar, A., & Chaudhry, A. (2009). Identification of Drought-Vulnerable Areas Using NOAA AVHRR Data. *International Journal of Remote Sensing*, 30(10), 2653-2668. <https://doi.org/10.1080/01431160802555788>
- Jensen, P., Krogsgaard, M. R., Christiansen, J., Brændstrup, O., Johansen, A., & Olsen, J. (1995). Observer Variability in the Assessment of Type and Dysplasia of Colorectal Adenomas, Analyzed Using Kappa Statistics. *Diseases of the colon & rectum*, 38(2), 195-198. <https://doi.org/10.1007/BF02052450>
- Kafy, A. A., Saha, M., Fattah, M. A., Rahman, M. T., Duti, B. M., Rahaman, Z. A., ... & Sattar, G. S. (2023). Integrating Forest Cover Change and Carbon Storage Dynamics: Leveraging Google Earth Engine and InVEST Model to Inform Conservation in Hilly Regions. *Ecological Indicators*, 152, 110374. <https://doi.org/10.1016/j.ecolind.2023.110374>
- Key, C. H., & Benson, N. C. (2006). Landscape assessment (LA). In: Lutes, D. C., Keane, R. E., Caratti, J. F., Key, C. H., Benson, N. C., Sutherland, S., Gangi, L. J. (Eds.). *FIREMON: Fire Effects Monitoring and Inventory System*. Gen. Tech. Rep. RMRS-GTR-164-CD. Fort Collins, CO: US Department of Agriculture, Forest Service, Rocky Mountain Research Station. p. LA-1-55, 164.
- Khan, R., & Gilani, H. (2021). Global Drought Monitoring with Drought Severity Index (DSI) Using Google Earth Engine. *Theoretical and Applied Climatology*, 146(1-2), 411-427. <https://doi.org/10.1007/s00704-021-03715-9>
- Kogan, F. N. (1995). Application of Vegetation Index and Brightness Temperature for Drought Detection. *Advances in Space Research*, 15(11), 91-100. [https://doi.org/10.1016/0273-1177\(95\)00079-T](https://doi.org/10.1016/0273-1177(95)00079-T)
- Kogan, F., & Sullivan, J. (1993). Development of Global Drought-Watch System Using NOAA/AVHRR Data. *Advances in Space Research*, 13(5), 219-222. [https://doi.org/10.1016/0273-1177\(93\)90548-P](https://doi.org/10.1016/0273-1177(93)90548-P)
- Konkathi, P., & Shetty, A. (2021). Inter Comparison of Post-Fire Burn Severity Indices of Landsat-8 and Sentinel-2 Imagery Using Google Earth Engine. *Earth Science Informatics*, 14(2), 645-653. <https://doi.org/10.1007/s12145-020-00566-2>
- Krishnan, S. P. T., & Gonzalez, J. L. U. (2015). *Building Your Next Big Thing with Google Cloud Platform: A Guide for Developers and Enterprise Architects*. Springer, 371 pp.
- Lan, Z., Su, Z., Guo, M., Alvarado, E., Guo, F., Hu, H., & Wang, G. (2021). Are Climate Factors Driving the Contemporary Wildfire Occurrence in China? *Forests*, 12(4), 392. <https://doi.org/10.3390/f12040392>
- Lasaponara, R., Proto, A. M., Aromando, A., Cardellini, G., Varela, V., & Danese, M. (2019). On the Mapping of Burned Areas and Burn Severity Using Self Organizing Map and Sentinel-2 Data. *IEEE Geoscience and Remote Sensing Letters*, 17(5), 854-858. <https://doi.org/10.1109/LGRS.2019.2934503>
- Li, F., Miao, Y., Feng, G., Yuan, F., Yue, S., Gao, X., ... & Chen, X. (2014). Improving Estimation of Summer Maize Nitrogen Status with Red Edge-Based Spectral Vegetation Indices. *Field Crops Research*, 157, 111-123. <https://doi.org/10.1016/j.fcr.2013.12.018>
- Li, W., Dong, R., Fu, H., Wang, J., Yu, L., & Gong, P. (2020). Integrating Google Earth Imagery with Landsat Data to Improve 30-M Resolution Land Cover Mapping. *Remote Sensing of Environment*, 237, 111563. <https://doi.org/10.1016/j.rse.2019.111563>

- Liao, T. W. (2005). Clustering of Time Series Data—A Survey. *Pattern Recognition*, 38(11), 1857-1874. <https://doi.org/10.1016/j.patcog.2005.01.025>
- Lin, L., Hao, Z., Post, C. J., Mikhailova, E. A., Yu, K., Yang, L., & Liu, J. (2020). Monitoring Land Cover Change on A Rapidly Urbanizing Island Using Google Earth Engine. *Applied Sciences*, 10(20), 7336. <https://doi.org/10.3390/app10207336>
- Liu, P. (2015). A Survey of Remote-Sensing Big Data. *Frontiers in Environmental Science*, 3, 45. <https://doi.org/10.3389/fenvs.2015.00045>
- Lopez, S., González, F., Llop, R., & Cuevas, J. M. (1991). An Evaluation of the Utility of NOAA AVHRR Images for Monitoring Forest Fire Risk in Spain. *International Journal of Remote Sensing*, 12(9), 1841-1851. <https://doi.org/10.1080/01431169108955213>
- Los, S. O., Pollack, N. H., Parriss, M. T., Collatz, G. J., Tucker, C. J., Sellers, P. J., ... & Dazlich, D. A. (2000). A Global 9-yr Biophysical Land Surface Dataset from NOAA AVHRR Data. *Journal of Hydrometeorology*, 1(2), 183-199. <https://doi.org/10.1175/1525-7541>
- Ma, Y., Wu, H., Wang, L., Huang, B., Ranjan, R., Zomaya, A., Jie, W. (2015). Remote Sensing Big Data Computing: Challenges and Opportunities. *Future Generation Computer Systems*, 51, 47-60. <https://doi.org/10.1016/j.future.2014.10.029>
- Mammadov, G. S., & Mammadov, M. I. (2016). Ecology Evaluation of Vineyard Soils Under the Condition of Ganja-Gazakh and Mountainous Shirvan Zone of Azerbaijan. *Annals of Agrarian Science*, 14(4), 343-345. <https://doi.org/10.1016/j.aasci.2016.10.007>
- Mehmood, H., Conway, C., & Perera, D. (2021). Mapping of Flood Areas Using Landsat with Google Earth Engine Cloud Platform. *Atmosphere*, 12(7), 866. <https://doi.org/10.3390/atmos12070866>
- Mellor, A., Haywood, A., Stone, C., & Jones, S. (2013). The Performance of Random Forests in an Operational Setting for Large Area Sclerophyll Forest Classification. *Remote Sensing*, 5(6), 2838-2856. <https://doi.org/10.3390/rs5062838>
- Minařík, R., & Langhammer, J. (2016). Use of A Multispectral UAV Photogrammetry for Detection And Tracking of Forest Disturbance Dynamics. *International Archives of the Photogrammetry, Remote Sensing & Spatial Information Sciences*, 41. <https://doi.org/10.5194/isprs-archives-XLI-B8-711-2016>
- Moharrami, M., Javanbakht, M., & Attarchi, S. (2021). Automatic Flood Detection Using Sentinel-1 Images on the Google Earth Engine. *Environmental Monitoring and Assessment*, 193, 1-17. <https://doi.org/10.1007/s10661-021-09037-7>
- Moore, R. T., & Hansen, M. C. (2011). Google Earth Engine: A New Cloud-Computing Platform for Global-Scale Earth Observation Data and Analysis. *American Geophysical Union, Fall Meeting Abstracts*, pp. IN43C-02.
- Na, X., Zhang, S., Li, X., Yu, H., & Liu, C. (2010). Improved Land Cover Mapping Using Random Forests Combined with Landsat Thematic Mapper Imagery and Ancillary Geographic Data. *Photogrammetric Engineering & Remote Sensing*, 76(7), 833-840. <https://doi.org/10.14358/PERS.76.7.833>
- Pal, M. (2005). Random Forest Classifier for Remote Sensing Classification. *International Journal of Remote Sensing*, 26(1), 217-222. <https://doi.org/10.1080/01431160412331269698>
- Parks, S. A., Holsinger, L. M., Voss, M. A., Loehman, R. A., & Robinson, N. P. (2018). Mean Composite Fire Severity Metrics Computed with Google Earth Engine Offer Improved Accuracy and Expanded Mapping Potential. *Remote Sensing*, 10(6), 879. <https://doi.org/10.3390/rs10060879>
- Rahman, A. M., Nemoto, K., Matsushima, K. I., Uddin, S. B., & AKM, G. (2022). A History of Cannabis (Ganja) as an Economic Crop in Bangladesh from the Late 18th Century to 1989. *Tropical Agriculture and Development*, 66(1), 21-32.
- Reinisch, E. C., Ziemann, A., Flynn, E. B., & Theiler, J. (2020). *Combining Multispectral Imagery and Synthetic Aperture Radar for Detecting Deforestation*. Algorithms, Technologies, and Applications for Multispectral and Hyperspectral Imagery XXVI (Vol. 11392, pp. 72-85). SPIE.
- Rezaei, M. M. H., Valizadeh, K. K., Rostamzadeh, H., & Rezaei, A. (2014). Assessing the Efficiency of Vegetation Indicators for Estimating Agricultural Drought Using MODIS Sensor Images (Case Study: Sharghi Azerbaijan Province). *International Journal of Advanced Biological and Biomedical Research*, 2(2), 399-407.
- Rosa, A. (2022). Importance and Role of Common Hazel (*Corylus avellana* L.) in Folk Medicine and Industry in Azerbaijan. *AGRIS - International System for Agricultural Science and Technology*, 8(11), 78-82.
- Rummukainen, M. (2012). Changes in Climate and Weather Extremes in the 21st Century. *Wiley Interdisciplinary Reviews: Climate Change*, 3(2), 115-129. <https://doi.org/10.1002/wcc.160>
- Rwanga, S. S., & Ndambuki, J. M. (2017). Accuracy Assessment of Land Use/Land Cover Classification Using Remote Sensing and GIS. *International Journal of Geosciences*, 8(04), 611. [10.4236/ijg.2017.84033](https://doi.org/10.4236/ijg.2017.84033)
- Sazib, N., Mladenova, I., & Bolten, J. (2018). Leveraging the Google Earth Engine for Drought Assessment Using Global Soil Moisture Data. *Remote sensing*, 10(8), 1265. <https://doi.org/10.3390/rs10081265>
- Scheip, C. M., & Wegmann, K. W. (2021). HazMapper: A Global Open-Source Natural Hazard Mapping Application in Google Earth Engine. *Natural Hazards and Earth System Sciences*, 21(5), 1495-1511. <https://doi.org/10.5194/nhess-21-1495-2021>
- Schmid, J. N. (2017). *Using Google Earth Engine for Landsat NDVI Time Series Analysis to Indicate the Present Status of Forest Stands*. [Dissertation Faculty of Geoscience and Geography of the Georg-August-Universität Göttingen.] Vol. 10, 39
- Seydi, S. T., Akhoondzadeh, M., Amani, M., & Mahdavi, S. (2021). Wildfire Damage Assessment over Australia Using Sentinel-2 Imagery and MODIS Land Cover Product within the Google Earth Engine Cloud Platform. *Remote Sensing*, 13(2), 220. <https://doi.org/10.3390/rs13020220>
- Sharifi, A., & Felegari, S. (2023). Remotely Sensed Normalized Difference Red-Edge Index for Rangeland Biomass Estimation. *Aircraft Engineering and Aerospace Technology*, 95, 1128-1136.
- Sheykhoumousa, M., Mahdianpari, M., Ghanbari, H., Mohammadimanes, F., Ghamisi, P., & Homayouni, S. (2020). Support Vector Machine Versus Random Forest for Remote Sensing Image Classification: A Meta-Analysis and Systematic Review. *IEEE Journal of Selected Topics in Applied Earth Observations and Remote Sensing*, 13, 6308-6325. <https://doi.org/10.1109/JSTARS.2020.3026724>
- Sidhu, N., Pebesma, E., & Câmara, G. (2018). Using Google Earth Engine To Detect Land Cover Change: Singapore as A Use Case. *European Journal of Remote Sensing*, 51(1), 486-500. <https://doi.org/10.1080/22797254.2018.1451782>
- Sim, J., & Wright, C. C. (2005). The Kappa Statistic in Reliability Studies: Use, Interpretation, and Sample Size Requirements. *Physical Therapy*, 85(3), 257-268. <https://doi.org/10.1093/ptj/85.3.257>
- Sui, C., Tian, Y., Xu, Y., & Xie, Y. (2014). Unsupervised Band Selection by Integrating the Overall Accuracy and Redundancy. *IEEE Geoscience and Remote Sensing Letters*, 12(1), 185-189. <https://doi.org/10.1109/LGRS.2014.2331674>
- Tavakkoli Piralilou, S., Einali, G., Ghorbanzadeh, O., Nachappa, T. G., Gholamnia, K., Blaschke, T., & Ghamisi, P. (2022). A Google Earth Engine Approach for Wildfire Susceptibility Prediction Fusion with Remote Sensing Data of Different Spatial Resolutions. *Remote sensing*, 14(3), 672. <https://doi.org/10.3390/rs14030672>
- Trenberth, K. E. (2011). Changes in Precipitation with Climate Change. *Climate Research*, 47(1-2), 123-138. <https://doi.org/10.3354/cr00953>
- Viera, A. J., & Garrett, J. M. (2005). Understanding Interobserver Agreement: the Kappa Statistic. *Family medicine*, 37(5), 360-363.
- Wang, D., Morton, D., Masek, J., Wu, A., Nagol, J., Xiong, X., ... & Wolfe, R. (2012). Impact of Sensor Degradation on the MODIS NDVI Time Series. *Remote Sensing of Environment*, 119, 55-61. <https://doi.org/10.1016/j.rse.2011.12.001>

- Yu, M., Yang, C., & Li, Y. (2018). Big Data in Natural Disaster Management: A Review. *Geosciences*, 8(5), 165. <https://doi.org/10.3390/geosciences8050165>
- Zhang, F., & Yang, X. (2020). Improving Land Cover Classification in an Urbanized Coastal Area by Random Forests: The Role of Variable Selection. *Remote Sensing of Environment*, 251, 112105. <https://doi.org/10.1016/j.rse.2020.112105>
- Zhao, Q., Yu, L., Li, X., Peng, D., Zhang, Y., & Gong, P. (2021). Progress and Trends in the Application of Google Earth and Google Earth Engine. *Remote Sensing*, 13(18), 3778. <https://doi.org/10.3390/rs13183778>
- Zhao, X., Xia, H., Liu, B., & Jiao, W. (2022). Spatiotemporal Comparison of Drought in Shaanxi–Gansu–Ningxia from 2003 to 2020 Using Various Drought Indices in Google Earth Engine. *Remote Sensing*, 14(7), 1570. <https://doi.org/10.3390/rs14071570>
- Zhao, X., Xia, H., Pan, L., Song, H., Niu, W., Wang, R., ... & Qin, Y. (2021). Drought Monitoring over Yellow River Basin from 2003–2019 Using Reconstructed MODIS Land Surface Temperature in Google Earth Engine. *Remote Sensing*, 13(18), 3748. <https://doi.org/10.3390/rs13183748>
- Zhong, F., Cheng, Q., & Wang, P. (2020). Meteorological Drought, Hydrological Drought, and NDVI in the Heihe River Basin, Northwest China: Evolution and Propagation. *Advances in Meteorology*, 2020, 1-26. <https://doi.org/10.1155/2020/2409068>